PCCP

PAPER

View Article Online
View Journal | View Issue

Cite this: *Phys. Chem. Chem. Phys.*, 2019, **21**, 7576

Electric charge of nanopatterned silica surfaces†

H. Gokberk Ozcelik and Murat Barisik *

Received 4th February 2019,
Accepted 13th March 2019

DOI: 10.1039/c9cp00706g

rsc.li/pccp

The most recent technologies employ nanoscale surface patterning or roughening in order to engineer desired properties on a surface. Electrokinetic properties at the interface of such surfaces and ionic liquids show different behavior to the well-known theoretical descriptions. Basically, the ionic distribution on the surface differs due to electrical double layer overlap effects in the pits and curvature effects at the tips of surface structures. Generally, the charge density of a surface is assumed to be a material property and surface roughness effects are overlooked in most of the literature. In contrast, we properly calculated the local surface charges based on surface chemistry at the corresponding local ionic concentration (charge regulation) for various surface roughness and solution conditions. The results showed that the surface charge density of silica decreased at the pits but increased at the tips of surface patterns. Even for the simplest case of self-repeating surface structures, the average of local surface charges becomes lower than the theoretical predictions. Based on numerical calculations, a phenomenological model was developed as an extension to the existing flat surface theory, which can successfully predict the average surface charge on a nano patterned surface as a function of the surface pattern size, ionic concentration and pH.

The electrostatic properties of surfaces play a key role in several recent nano-technologies. When a solid surface meets an aqueous medium, molecular surface groups interact with the ionic fluid and form a chemical equilibrium defining the charge property of the solid surfaces. This surface charge determines the interactions and transport in nano systems, including particle transport in nanofluidic devices,[1] separation processes such as desalination,[2,3] measurement of surface topography,[4,5] drug delivery,[6,7] DNA and protein transport,[8,9] and biological/chemical agent detection.[10,11] The design and performance of these applications requires an accurate knowledge of surface charging mechanisms at various conditions, which are not yet well understood.

Surface charge originates from reactions occurring at the interfaces between an immersed body and an electrolyte solution.[12] The association/disassociation of polar groups and the adsorption of ions creates the surface charge based on solution properties such as the electrolyte concentration, pH and variety of ions. The charged interface attracts counter ions and forms an electric double layer (EDL).[13] In such a context, the surface charge and EDL are interrelated; one forms the other. In general, the ionic distribution on the surface is described by the Boltzmann distribution (BD) by assuming a flat surface sufficiently away from any other bodies. After further simplifications, the electric charge of the corresponding surface is calculated analytically. Many existing studies and applications use such an approach and assume a constant charge density on a surface calculated for the corresponding material. However, the flat surface assumption is very much against the nature shown by a variety of surface topologies where the ionic distribution on the surface and the resulting electric charge will be different from the BD based descriptions. Assuming surface roughness or patterns in the form of hills and valleys on nano-scales, divergence from the BD develops in two ways for a non-planar surface. First, for valley spacings comparable with or smaller than the thickness of the EDL, ionic layers (EDLs) extending from opposite surfaces overlap, causing the local ionic concentrations to differ from the BD. Second, for hill sizes comparable with or smaller than the thickness of the EDL, curvature effects develop due to the decreased surface to volume ratio, creating an ionic distribution different to the BD again. The curvature effect has been observed by multiple researchers in the surface charge behavior of nano-particles.[14,15] These two occurrences yield local variation of the surface charge as a function of the surface nano topology, which was observed by a few studies through AFM measurements[16] and numerical simulations,[17,18] but there has not been any proper characterization of the behavior, yet.

A non-homogenous distribution of the charge of a surface can be used to create many interesting mechanisms. The modification of the surface charge distribution or surface charge patterning at the nano-scale is exercised in a wide range of applications, such as creating anti-bacterial surfaces,[19,20] controlling the thermodynamic phase behavior of colloids,[21,22] designing the

Department of Mechanical Engineering, Izmir Institute of Technology, IZMIR, 35430, Turkey. E-mail: muratbarisik@iyte.edu.tr

† Electronic supplementary information (ESI) available: Additional details of chemical models and calculations. See DOI: 10.1039/c9cp00706g

behavior of nanoparticles,[23,24] controlling fluid flow and mixing in Lab-on-a-chip devices,[25,26] developing desired Janus particles,[27] controlling cell microenvironments,[28,29] or even mimicking organ behaviors in organ-on-a-chip devices.[30] However, nano-patterned surface charges are frequently developed using very sophisticated and complicated techniques such as positioning charge or nano patterns using AFM[31] and optical tweezers,[32] or controlling self-assembly of biological/chemical groups[33] and nanoparticles.[34] Instead, the manipulation of local surface charge can be obtained by simply changing the surface topography. The alteration of the surface topography or surface patterning was originally employed to modify the interfacial energy for the control of wetting, heat transfer and fluid transport. For example, the wetting of a surface can be changed depending on the size and geometry of the structures formed on the surface; hydrophobic behavior can be created for self-cleaning or anti-icing surfaces,[35] while a hydrophilic surface can be obtained for more efficient biomedical or heat transfer applications.[36] Since surface patterning is employed by larger communities, the fabrication techniques are more established. Nanolithography can be used to construct desired structures or chemical etching can be used to develop fractal structures or femtosecond lasers can be used to ablate surface patterns. The latter approach, becoming popular just recently, is very promising due to its flexibility, simplicity, and controllability in creating several types of nano/microstructures required for a wide range of applications. Manipulation of surface charge by changing the surface topography was utilized recently by creating fractal structures as an electrode for enhanced electrophoresis properties[37] and efficiency in detecting biomolecules.[38] But, there is not a proper correlation between the surface topography and the surface charge. Although surface patterning is a well-known approach to tune the surface properties of materials in wide range of applications, there is a gap to link the local surface charge properties to surface patterning because physical heterogeneity is not the only complication, local complications originating from physical heterogeneity such as overlapping of EDLs, curvature, and size effects of asperities should also be considered.

It is also important to mention that one of the most common nanotechnology applications determines the topology of a surface under an ionic fluid by measuring the electrostatic pressure forces on the surface developed from surface charges. The well-known Atomic Force Microscope (AFM) post-processes measured force *vs.* distance curves over a certain point of a substrate to determine the surface location generally using the classical DLVO theory (developed by Derjaguin & Landau[39] and Verwey & Overbeek[40,41]). DLVO describes the interaction force between charged surfaces in a liquid medium by formulizing the two main components of interparticle interaction, van der Waals and EDL forces, based on the BD assuming a planar surface. The presence of surface structural variations leads to secondary interactions which can be included by the updated DLVO calculations.[42–44] However, these extensions consider roughness effects as a physical heterogeneity and continued to employ the homogenous surface charge assumption. On the contrary, the presence of roughness triggers further complications in the surface chemistry due to the local ionic variation originating from the EDL overlap in the pits and the curvature effects at the tips of the surface structure. Most of the existing AFM calculations disregard this surface charge heterogeneity, which can be attributed to the lack of a simple approach to characterize the variation in the surface charge with the surface topography. Only recently, a few AFM studies have underlined this discrepancy and questioned the determination of the location of the surface based on the constant[45,46] and homogenous[16] surface charge assumption; instead, they recommended extending the DLVO theory to consider the so-called "Charge Regulation (CR)" nature of the surface chemistry.[47] CR was first identified by Ninham and Parsegian[48] and later observed in multiple studies by surface force measurements on colloids[49,50] and AFM.[4,51,52] These studies were conducted on perfectly planar surfaces with a known surface location and force measurements were used to determine the surface charge, contrary to the classical approach of a known surface charge and an unknown surface location. Through these studies, the CR was mostly considered for the variation of the surface charge at a specific surface location due the EDL overlap between the AFM tip and the surface at various separation distances during an AFM force measurement. There are only limited studies considering the surface charge heterogeneity, but even these do not properly characterize or offer an explicit solution for the surface charge behavior of non-planar surfaces.

Other than the AFM literature, calculations of the surface charge density as a function of the local ionic environment have been practiced for nanoscale confinement. The numerical solution of the ionic distributions is coupled with the CR models as a surface boundary condition. The CR models calculate the effects of the protonation/deprotonation in surface reactions based on the site density of the functional groups. Most of the existing literature focuses on the surface charging characteristics of straight channels[53–55] and tubes[56,57] where EDLs overlap and entrance/exit effects create local variation of the surface charge on planar surfaces. There are only a few studies in the literature that refer to the surface topology effect on surface charging,[16–18] but these studies presented their results without examining or describing its occurrence. Hence, there has not been a proper characterization or explicit solution for the surface charge behavior of non-planar surfaces, yet.

The aim of this work is to investigate the surface charge density of nano-patterned silica surfaces as a function of the pattern size at various solution conditions. Silica is chosen due to its widespread application uses in colloidal science, drug delivery and nanofluidic studies. Previously proposed analytical methods for surface charge calculations are restricted due to the employed Debye–Hückel approximation, which is applicable only for low surface charge values. Instead, finite element based multiphysics simulations are employed with a multi-ion charge-regulation model[15,58] to solve the Poisson–Nernst–Planck equation to consider the effects of EDL overlap and curvature on a patterned surface for the first time in the literature.

Theoretical background and mathematical model

In general, the ionic distribution on a surface with a given surface charge density obeys the Boltzmann distribution (BD)[59,60] and the potential distribution through a semi-infinite EDL can be calculated by the well-known Poisson–Boltzmann (PB) equation. The Debye–Hückel simplification[61] yields an analytical solution of the PB equation for low wall potentials (<25 mV). The high wall potential cases require the solution of complex elliptic functions[62,63] or use of trial error methods to calculate the electric potential.[64,65] However, all these methods are only valid for semi-infinitely extending EDL fields. In the case of EDL overlap where the EDLs growing from opposite surfaces start interacting, using the Boltzmann distribution in the Poisson equation becomes incorrect.[53,64] The potential distribution with EDL overlap significantly deviates from the no-overlap cases obeying the Boltzmann distribution. For such a case, the original form of the Poisson–Nernst–Planck (PNP) theory should be employed in the analyses, in contrast to frequently used simplified versions of PNP.[59,66] Defining the surface boundary condition in the case of EDL overlap also requires additional attention. In most of the literature, assigning either a constant surface charge[67,68] or constant wall potential[69] boundary condition onto the surfaces is the general way to solve PNP. The wall potential (ψ) and surface charge density on the wall (σ_w) are related to each other as given in eqn (1). If a constant surface charge density is assumed on overlapping surfaces, the electric potential value at the surface will change by EDL overlap. On the other hand, if a constant wall potential condition is implied, EDL overlap will cause the change of the surface charge density (*i.e.* the slope of the potential distribution at the wall). These cases are common practices in the existing literature,[44] however, both approaches do not properly reproduce the nature of the surface.

$$-\varepsilon_0\varepsilon_r\vec{n}\cdot\nabla\Psi = \sigma_w \quad (1)$$

Enforcing a constant surface charge or potential at the interface does not represent the physical response of the surface chemistry. Surface reactions develop based on the local ionic environment at the interface and neither the surface charge nor the potential remain constant; instead, both of them undergo variation in response to the variation in the ionic distribution and create a new equilibrium, accordingly. Such behavior is modelled by the previously developed multi-ion charge-regulation model, which considers the effects of the protonation/deprotonation surface reactions, the site density of the functional groups, and the pH & salt concentration of the aqueous solution on the silica surface. This boundary condition model forms the basis of the current study.

In the current model, a silica surface with spherical nano patterns with diameter D_R is considered as illustrated in Fig. S1 (ESI†). The liquid phase is a KCl (*i.e.* symmetric 1 : 1) aqueous electrolyte solution consisting of 4 types of ionic species, namely H^+, K^+, Cl^- and OH^- ions, with their bulk values being c_{10}, c_{20}, c_{30} and c_{40}, respectively. Due to protonation/deprotonation of ions, the silica surface is charged when in contact with an ionic solution. The surface charge is mainly controlled by the K^+ and Cl^- ions while the pH of the solution is adjusted by the H^+ and OH^- ions. Detailed information on the Poisson–Nernst–Plank (PNP) equations employed in the study is given in the ESI.†

Due to the protonation/deprotonation reactions at the solid/liquid interface, the silica channel walls show a charge-regulated behavior depending on the ionic concentration and pH of the ionic aqueous solution. In order to implement this charge regulated nature into the model, two fundamental dissociation/association reactions are considered to be occurring at the solid/liquid interface as follows:

$$SiOH \leftrightarrow SiO^- + H^+ \quad (2)$$

$$SiOH + H^+ \leftrightarrow SiOH_2^+ \quad (3)$$

The equilibrium constants are evaluated by using

$$K_A = \frac{\Gamma_{SiO^-}[H^+]_w}{\Gamma_{SiOH}},\ K_B = \frac{\Gamma_{SiOH_2^+}}{\Gamma_{SiOH}[H^+]_w} \quad (4)$$

where Γ_{SiO^-}, Γ_{SiOH} and $\Gamma_{SiOH_2^+}$ are the surface site densities of SiO^-, SiOH and $SiOH_2^+$, respectively, and $[H^+]_w$ is the hydrogen concentration at the solid/liquid interface. In this regard, the surface charge density of the silica walls can be denoted as:

$$\sigma_w = -\frac{F\Gamma_{total}}{N_A}\frac{K_A - K_B[H^+]_w^2}{K_A + [H^+]_w + K_B[H^+]_w^2} \quad (5)$$

Eqn (5) basically determines the difference in the number of charged sites (SiO^- and $SiOH_2^+$) at the final equilibrium of the dissociation/association reaction developing on the surface at the corresponding ionic conditions. Similar 2-pK models for dissociation and association reactions have been implemented in the literature for many years due to their success in capturing the titration behavior of aqueous silica surfaces.[70] Later, direct measurements of such charging sites were accomplished. One of the very first studies to offer proof of surface groups at the silica water interface was done by investigating the oxidation states of surface atoms *via* XPS measurements.[71] Both O 1s spectra[71] and Si 2p spectra[72] from silica XPS measurements exhibit pH dependent behavior in the electron binding energy. Moreover, increasing surface charge with increasing pH described by the charge regulation models was also validated by these experiments.

Results

Our investigations began by calculating the ionic distribution over surfaces with a roughness diameter (D_R) of 1 nm, 5 nm and 10 nm. The ionic concentration was varied as C_{KCl} = 1 mM, 10 mM and 100 mM, while the pH was kept constant at 6. Fig. 1 presents the electric potential contours of all these cases; each row is the same salt concentration and each column is the same roughness diameter. First, a decrease in salt concentration (*i.e.*; from the third row to the first row) increases the thickness

of the EDL such that EDLs growing from facing surfaces of nano-patterns overlap. EDL thickness values smaller than D_R create no overlap and the local ionic concentration through the surface remains constant (*i.e.*; D_R = 5 nm and 20 nm at C_{KCl} = 1 mM or D_R = 20 nm at C_{KCl} = 10 mM). However, when the EDL thickness becomes equal to or higher than D_R, a non-homogenous potential distribution develops on the surface. Here, the EDL thickness (λ) normalized with D_R appeared as a proper representation of the degree of EDL overlap on the surface. Overlapping is initially observed at the bottom of cavities, then as λ/D_R increases, overlapping spreads to the top of cavities. When the overlapping extends over patterns, the bumpy potential distribution on the surface becomes rather flat in the lateral direction.

Next, we calculated the local surface charge densities based on the ionic potential formed on the surface. Fig. 2 gives the distribution of surface charge on the surfaces given in Fig. 1 along the normalized lateral position (x/D_R). The averaged surface charge density (average of local values) and the PB calculated surface charge density of a flat surface for the same pH and salt concentrations are also given for each case. Different surface charge values develop at different bulk ion concentrations. First, for low λ values with high D_R creating low λ/D_R values, the charge is almost constant on the surface and the average surface charge is similar to the prediction of flat surface theory. For instance, there is no interaction between EDLs when D_R = 20 nm at 10 mM and 100 mM, presented in Fig. 1(f and i), and the surface charge densities given in Fig. 2(f and i) show only slight variation due to the weak curvature effects on the patterns. However, the increase of λ and/or decrease of D_R yield EDL overlap and stronger curvature effects such that the surface charge shows distinct local variations and the average surface charge of the nano-patterned surface becomes different to the flat surface calculations. Even though the curvature effect increases the absolute value of the surface charge as the diameter is decreased,[15] EDL overlap decreasing the absolute charge dominates and the average surface charge becomes lower than the absolute charge of a flat surface.

In order to characterize the local charge variation on the nano-patterns, we performed calculations for a wide range of roughness diameters between 1 nm and 40 nm. Specifically, we measured the local surface charge at the tip and the dip of the surface pattern in the form of half circles. For comparison, we also calculated the surface charge of nanoparticles, as described in another study,[15] at the diameter values of the surface roughness. Surface charge results normalized with the theory of a flat surface at the corresponding conditions are given in Fig. 3 for different salt concentrations of (a) 100 mM, (b) 10 mM and (c) 1 mM. As a first observation, surface charges measured at the tips of the rough surface were found to be identical to the surface charge of a nanoparticle with the same diameter, except in the overlapped cases. Depending on the ionic concentration, EDL overlap develops at different roughness diameters, at which the charging behavior on the tip differs from nanoparticle charge behavior. Basically, the nanoparticle and the tip of the surface roughness are almost identical up to diameter of 2 nm for the lowest EDL thickness developed in the 100 mM case, while the divergence in the 1 mM case starts for diameters smaller than 10 nm. Overall, the absolute value of surface charge values at the tip is higher than the flat surface predictions and increases with the decrease of the surface roughness. Second, the surface charge developing at the dip of the valleys showed the opposite behavior such that the absolute surface charge was lower than the flat surface and decreased as the roughness diameter decreased. Interestingly, these high and low values cancel each other out so that the average surface charge becomes similar to the flat surface charge up to certain roughness diameters. With the development of EDL overlap governed by both the surface roughness and EDL thickness, the absolute value of the average surface charge diverges from flat surface calculations.

Further characterization based on the overlap ratio (λ/D_R) is performed as a function of pH. In Fig. 4(a), the surface charge density on the top of the surface pattern normalized by the surface charge of the nanoparticle at the same diameter as the roughness is presented as a function of pH at different overlap

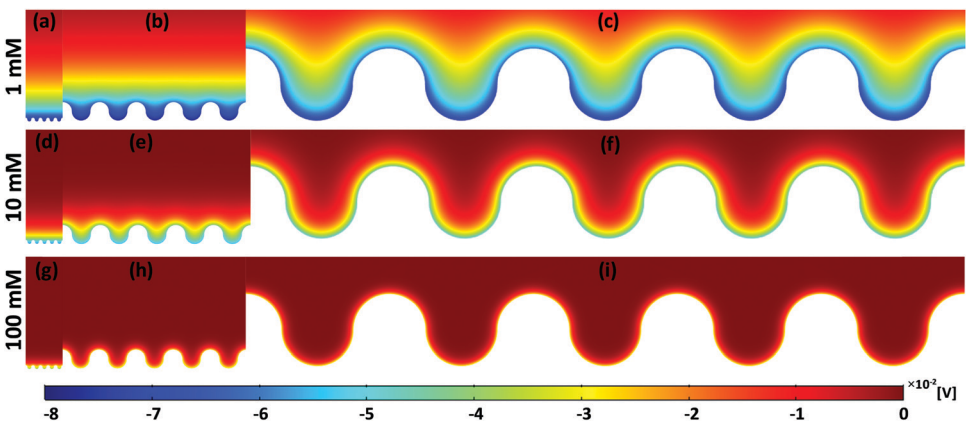

Fig. 1 Potential distributions of different concentrations and roughness diameters at pH = 6. The (a, g and d), (b, e and h) and (c, f and i) cases have 1 nm, 5 nm and 20 nm diameter roughness values, while the (a, b and c), (d, e and f) and (g, h and i) cases represent 1 mM, 10 mM and 100 mM salt concentrations, respectively.

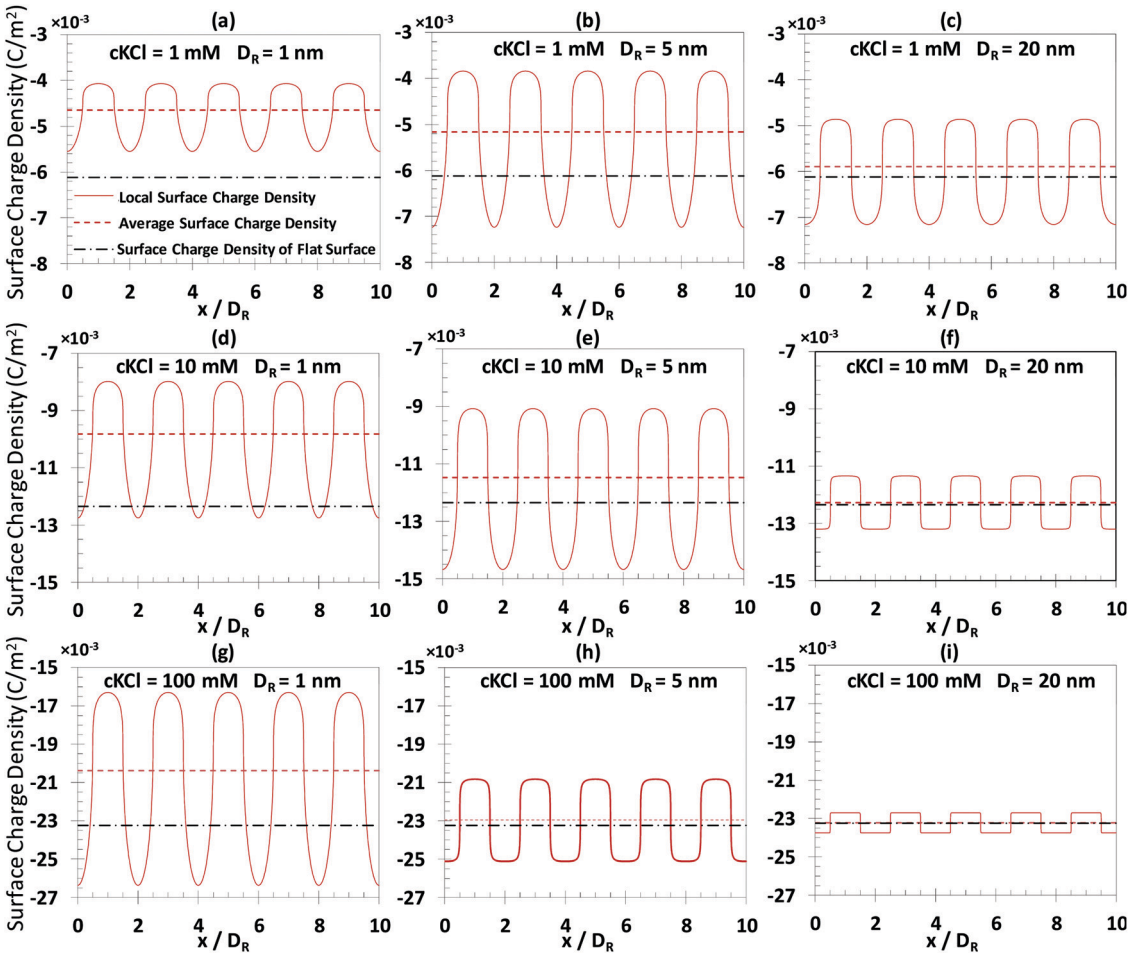

Fig. 2 Surface charge density distribution over different rough surfaces at different concentrations (at pH = 6). The (a, g and d), (b, e and h) and (c, f and i) cases have 1 nm, 5 nm and 20 nm diameter roughness values, while the (a, b and c), (d, e and f) and (g, h and i) cases represent 1 mM, 10 mM and 100 mM salt concentrations, respectively.

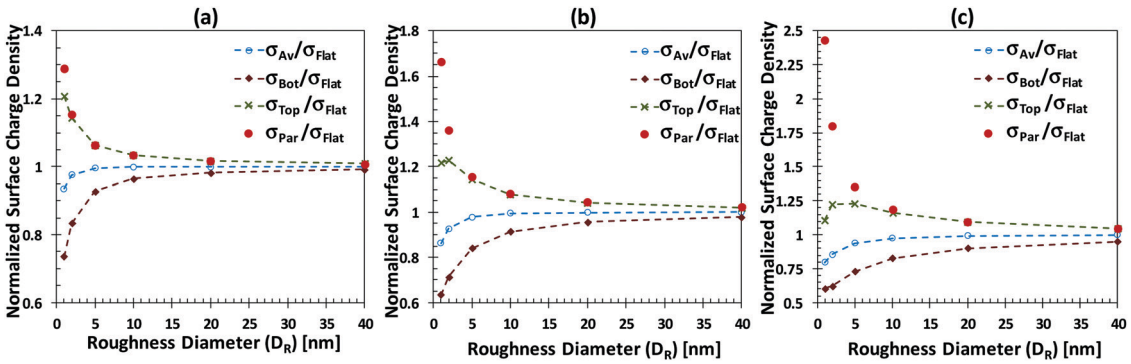

Fig. 3 Normalized local charge densities measured on the top and bottom of surface patterns for different roughness diameters accompanied by the average surface charge at the (a) 100 mM, (b) 10 mM and (c) 1 mM salt concentrations.

ratios. Curvature effects observed on surface pattern tips create surface charge values very similar to the nanoparticles' surface charge up to λ/D_R = 0.5 after which overlap growing from the dips alters the surface charge on the tips. As the overlap ratio increases, the tip charge becomes lower than the nanoparticle counterpart at different levels depending on the pH. Negligible divergence develops at low pH values regardless of the overlap ratio; moderate effects are observed for pH values higher than 4, after which an increase of pH enhances the divergence up to pH = 6 and then the divergence decreases again. A comparison of the tip charge with the flat surface charge is given in Fig. 4(b) for different overlap ratios and

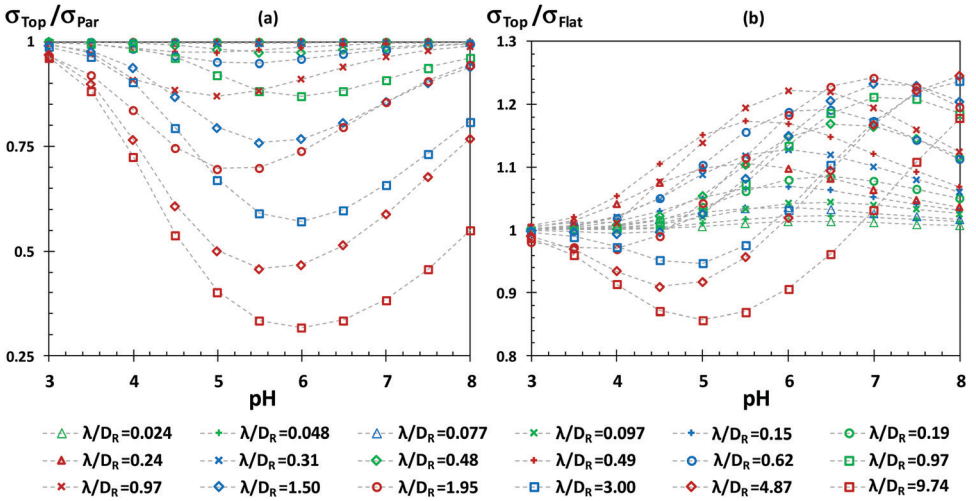

Fig. 4 Variation of the surface charge density on the top of the surface pattern compared to (a) the particle at the diameter of the corresponding roughness and (b) the flat surface as a function of pH.

pH values. In the absence of EDL overlap at low overlap ratios, the surface charge under curvature effects becomes higher than the flat surface. The behavior observed for $\lambda/D_R < 0.5$ is similar to results from the literature.[15] The increase of overlap results in a decrease of the tip charge, reaching the flat surface value and going below for low pH values, while at high pH values (pH > 7) the tip charge remained higher than the flat surface.

We extended our investigation to the joint behavior of the tip and dip surface charging, and their average. As the surface reactions are governed by the concentration of hydrogen ions (H) on the surface, Fig. S3 (ESI†) focuses on the surface H concentrations normalized by the flat surface value at the corresponding pH, as a function of the overlap ratio and pH. To improve the readability, the results of pH = 3–5.5 and pH = 5.5–8 are plotted on two separate graphs. The silica surface develops negative charge between pH = 3 and pH = 8 silica, the high H concentrations create more protonation resulting in lower absolute surface charges. Two different trends are observed in the general behavior of the H concentration at both the top and bottom of the pattern. First, the H concentration at the bottom decreases with an increase of the overlap ratio up to a certain overlap ratio depending on the pH; then the trend completely changes and the H concentration increases as the overlap increases. The exact opposite behavior is observed on the bottom of the pattern. By combining these two behaviors, the average surface charge increases and reaches a constant with the increase of overlap. Overall, the variation of the average surface chemistry stops for $\lambda/D_R > 10$ depending on the pH value.

The average surface charges measured on nano-patterned surfaces at different roughness diameters, ionic concentrations, and pH values are summarized in Fig. 5. The general behavior shows a decrease in the patterned surface charge from the flat surface calculations starting from $\lambda/D_R = 0.2$ and higher while the nano-roughness mostly becomes effective for $\lambda/D_R > 0.5$. The average surface charge becomes independent of the surface roughness for high overlaps depending on the pH of the environment. This behavior develops very early in low pH cases ($\lambda/D_R = 2$ for pH < 4.5), but moves further to higher $\lambda/D_R > 2$ with the increase of pH. Independent of the salt concentration, the divergence from theory increases as the pH increases. The charge of the patterned surface decreases to 3/4 of the flat surface value at $\lambda/D_R > 10$ and pH > 6. Overall, the average surface charge density varies between two asymptotes which are at the two limits of surface roughness.

In Fig. 5, the average surface charge as a function of the overlap ratio shows different behavior depending on the ionic concentration and pH. For such a case, it was challenging to normalize this charging behavior by the ionic properties. However, we also observed that there are certain cases of different salt concentration and pH showing matching variation with the change in overlap. For instance, 1 mM at pH = 4, 10 mM at pH = 4.5 and 100 mM at pH = 5 develop similar average surface charge values as a function of the overlap ratio. To characterize this behavior better, we convert the results onto

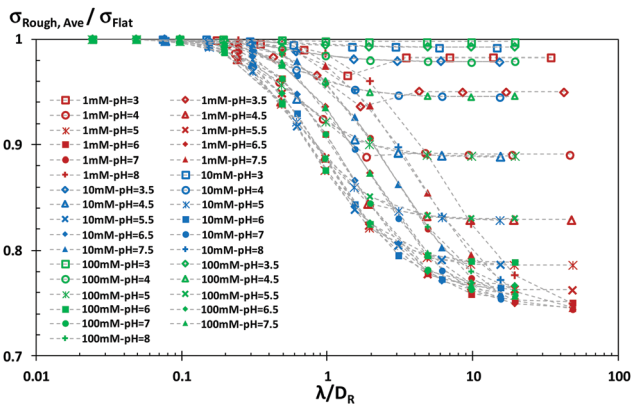

Fig. 5 Normalized average surface charge density on the nano-patterned surfaces at different roughness diameters, ionic concentrations, and pH values as a function of the overlap ratio.

the pH axis in Fig. S4 (ESI†). Overall, the u-shaped pH dependence shifts from left to right as the overlap increases. For high overlap ratios $\lambda/D_R > 10$, surface charging becomes pH independent for pH values higher than 5.5.

Next, we debated the effective boundary definition for the electrostatic properties over a rough surface. The effective boundary condition (BC) at a rough surface was investigated for fluid dynamics by many researchers,[73–75] but the electric BC on a rough surface is mostly overlooked by the literature. As the roughness diameter decreases, surface structures become negligible and the surface becomes almost flat. We observed this behavior through the potential distributions given earlier in Fig. 1, where the electric potential developed over small surface roughness (Fig. 1(a), (d) and (g)) shows a smooth distribution. The electric properties over a surface are not the result of surface roughness only, instead they are formed by the ratio of the EDL thickness to the surface roughness. Hence, electric potentials are flattened even at moderate surface roughness at high overlap ratios as can be seen from Fig. 1(b). Furthermore, any electrostatic or electrokinetic interaction between an object and a rough/patterned surface would be governed by the electric properties at the effective boundary region rather than the electric charge at the bottom of surface patterns. Based on this perspective, we studied the average electric potential measured through a line passing through the tips of the pattern parallel to the surface. The average electric potential measured on the tip line BC at different roughness diameters, ionic concentrations, and pH values is given in Fig. 6. These are the same cases at which surface charge values were calculated in the earlier Fig. 5 through the surface arc length path. The average electric potential on the top BC of the nanopatterns normalized with the flat surface potential increases with the increase of the overlap ratio; starting from zero potential at $\lambda/D_R \to 0$, the tip line BC reaches flat surface theory and remains constant for $\lambda/D_R > 10$. This is very interesting and expected behavior. Very low λ/D_R makes the tip line BC remain in the bulk of the EDL where negative and positive ions are at equal number, creating a zero-net electric potential. On the other end, high λ/D_R results in a flattened surface and surface potential and roughness effects disappear, and surface charging behaves almost like a flat surface, except the pH dependence. Let's remember that normalization is done by the flat surface value at the corresponding pH. At low λ/D_R values ($\lambda/D_R < 0.5$), the pH dependence of the tip line BC is very similar to flat surfaces in that all results remain on the same line. However, with the increase of λ/D_R, the potential values show a variation with the change of pH. Results at different ionic concentrations continue to show very similar behavior, which shows that ionic concentration effects were successfully normalized by the λ/D_R definition. At high λ/D_R values, high pH values gave identical results to the flat surface, but low pH created higher potential values than the flat surface calculations.

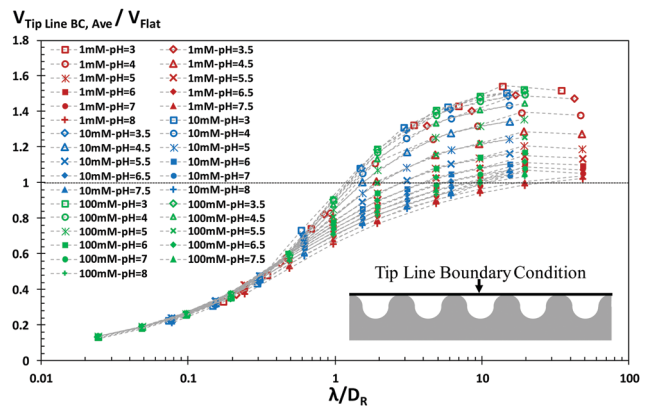

Fig. 6 Normalized average surface potential on the nano-patterned surfaces at different roughness diameters, ionic concentrations, and pH values as a function of the overlap ratio.

We further studied the pH dependence of the boundary potential in Fig. S5 (ESI†), presenting the normalized boundary potential as a function of pH. There was no significant pH dependence on the boundary potential observed up to $\lambda/D_R = 1$ and the potential remains as a constant flat line in Fig. S5 (ESI†). For higher overlap ratios ($\lambda/D_R > 1$), the normalized boundary potential increases with the decrease in pH.

In an attempt to provide an easy to use phenomenological model, we developed an empirical model as a fit to our numerical results. In this context, we found eqn (6) from the trigonometric functions family to be the best fit for the observed variation of the surface charge with the variation of the overlap ratio. As $\lambda/D_R \to 0$, eqn (6) has the value of unity representing the cases of negligible overlap where the surface charge on a rough surface is equal to the theoretical predictions. At the other end where $\lambda/D_R \to \infty$, eqn (6) approaches $1 - a$, as the parameter a accounts for the variation from the theory. Therefore, eqn (6) can simply model the variation of the normalized charge of rough surfaces between the two asymptotes of 1 and $1 - a$, while the surface charge values in between develop as a function of the overlap ratio and parameter b.

$$\frac{\sigma_{\text{Rough,Ave}}}{\sigma_{\text{Flat}}} = 1 - a\frac{b(\lambda/D_R)^2}{b(\lambda/D_R)^2 + 1} \tag{6}$$

The two parameters of eqn (6), a and b, depend on the pH and salt concentration of the ionic solution. Next, we studied the variation of these parameters by fitting eqn (6) to all of the calculations in Fig. S6 (ESI†). The a and b parameters showed variation between two asymptotes with opposite behavior and the hyperbolic trigonometric functions given in eqn (7) and (8) are able to provide a universal description for all of the studied cases.

$$a = \frac{pK_A - pK_B}{40}\left[1 + \text{Tanh}\left(\text{pH} - pK_A + pK_B - \frac{\log[\text{KCl}] - 1}{2}\right)\right] \tag{7}$$

$$b = \frac{pK_A - pK_B}{4}\left[1 - \text{Tanh}\left(\text{pH} - pK_A + pK_B - \frac{\log[\text{KCl}] - 4}{2}\right)\right] \tag{8}$$

The predictions of eqn (6) using eqn (7) and (8) showed very good agreement with the numerical results. In Fig. 7, the

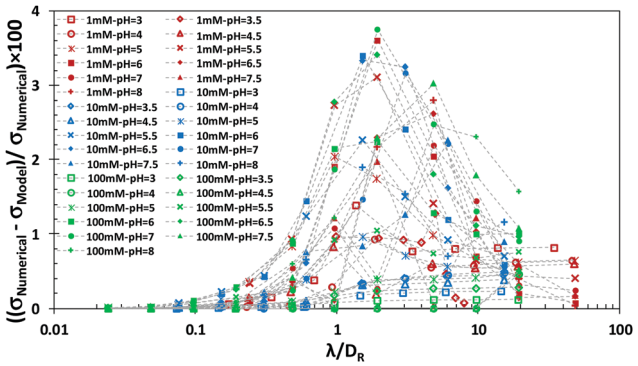

Fig. 7 Percentile of the relative error between the surface charge predictions of the empirical model (eqn (6)–(8)) and numerical results at different roughness diameters, ionic concentrations, and pH.

relative errors between our empirical model and the numerical results are shown for all cases as a function of the overlap ratio. Overall, there is no more than 4% difference between the empirical model and the numerical calculations. For overlap ratios less than 0.1 where surface roughness effects are negligible, our model can capture flat surface theory very precisely with a relative error of less than 0.2%. With the increase of the overlap ratio, the relative error shows variation case by case, but the average relative error of our model remains less than 1%. Hence, the proposed model successfully predicts the deviation of the surface charge density due to roughness effects as an extension to flat surface theory. It is important to mention that flat surface theory and so this new extension model are applicable to cases where the continuum assumption remains valid. This means D_R values less than certain scales ($D_R < \sim 1$ nm) cannot be predicted by PNP or by our model (eqn (6)). We should also note that this model calculates the average surface charge through the arc length path of the surface roughness; however, Fig. 6 suggests that as the overlap ratio approaches 10 ($\lambda/D_R \rightarrow 10$), the electric potential on rough surfaces flattens and the surface potential expected to be physically effective on a surface with low DR approaches back to flat surface value.

Discussion

A representative nano-patterned surface in the form of repeating concave and convex circles is studied due to two advantages. First, we can control the surface structures by varying the single quantity, D_R, and perform a parametric study by systematically varying it. Second, since the tip of the circles developed a curvature effect similar to nanoparticles, we can validate our calculations with our earlier work on nanoparticles,[19] which was validated by experiments. Until the overlap effects growing from the pits dominate, nanopattern tip surface charges with decreasing size are identical to the surface charge of the nanoparticle at the corresponding size.

Overall, surface electric charging on a nano-patterned surface is equal to the charge of a flat surface until the size of the structure becomes comparable with the corresponding EDL thickness. We characterized such formations using the non-dimensional Debye length definition, which was employed to investigate non-uniform behavior of surface electrostatics by many researchers in various forms, such as normalized by the particle diameter (λ/D_p),[15] distance between the particle and the surface (λ/h),[58] channel length (λ/L)[76] and channel height (λ/H).[76] For our case, the ratio of the EDL thickness to the roughness diameter as λ/D_R could represent both curvature effects on the tips and overlap effects in the pits of the roughness. Both of these effects creating divergence from regular flat surface theory develop with the decrease of the nano-pattern size represented by the roughness diameter or by the increase of the EDL thickness. For such cases, comparable variation of D_R and λ defines the surface charging and a very small D_R with a very small λ and a moderately small D_R with a moderately small λ create similar behaviors. λ/D_R offers insight about the general trend, which can be divided into three behaviors: with the increase of λ/D_R, (i) a slight divergence from the flat surface charge value, (ii) a significant increase up to a maximum deviation, and (iii) remaining constant at this maximum value. The general mechanisms can be explained as follows: initially, for a high salt concentration and for a high roughness diameter ($\lambda/D_R \rightarrow 0$), a diffuse layer can form completely parallel to the surface morphology and the rough surface develops flat surface electrostatics. As the thickness of the diffuse layer increases (or the roughness diameter decreases), first, overlap occurs at the bottom of surface structures, increasing the potential and causing more protonation and decreasing the absolute surface charge. Second, curvature effects develop at the tip of structures, decreasing the potential and protonation, which increases the absolute surface charge. Interestingly, for low λ/D_R values, these two cancel each other out until the overlap growing with the increasing λ/D_R dominates and decreases the average surface charge values on the nano-patterned surface.

Further characterization is required to determine the physically effective charge on the patterned surface for high λ/D_R cases. High λ/D_R for either small surface patterns or big EDL thicknesses repress the local variation on the patterned surface such that the potential distribution becomes almost flat. This simply suggests that surface heterogeneity effects on electrokinetics almost disappear for high λ/D_R. Especially for small pattern sizes, interaction on the nano-patterned surface should not be expected to develop through the electrostatic properties deep inside the pits of the patterns, instead effective electrokinetics will be governed by the properties through a region on the top of the surface patterns. For such a case, the tip line boundary condition is an idea to approach this behavior. Since we are not on a surface, we measured the electric potential instead of a charge value on the effective line BC. The variation of the electric potential on the line BC with the variation of λ/D_R is different to the behavior of the surface charge measured through the arc length of surface patterns. Simply, at low λ/D_R values, ionic accumulation (EDL) is mostly confined inside the nano-patterns such that the average potential on the tip line BC is almost zero; for these cases the current line BC may not be appropriate. For instance, for large D_R cases, electrokinetic

interactions are expected to develop through the arc length of surface patterns, not through the tip line BC. By increasing λ/D_R, ionic layering grows out of surface patterns such that the average potential at the tip line increases. First, it reaches a flat surface potential and then a constant value equal to or higher than the flat surface potential depending on the pH value. For example, at pH = 8, the tip line potential measured at different salt concentrations reaches the flat surface potential and remains constant with the increase of λ/D_R. However, lower pH values exceed the flat surface potential. This specific behavior is mostly attributed to the difference between the pH dependence of the potential on a surface and the potential on a line BC. In general, comparisons (or normalizations) are done by the flat surface value at the corresponding pH value. With the decrease of pH, the flat surface potential decreases while the tip line potential decreases more slowly; hence, at low pH values the tip line potential becomes higher than the flat surface potential.

As a final remark, the current calculations are based on the continuum approximation, which is not valid at certain nanoscale limits. The primary surface charging develops on the binding sites, which are usually described by the site density per area. While different experimental procedures reported different results, the site density for silica is mostly measured between 5 and 11 sites per nm^2.[77] There are positively and negatively charged surface groups distributed on these binding sites and the continuum description of the corresponding surface charge is approximated by the average of these surface groups. Such an average definition will not be appropriate for small bodies since there will not be enough binding sites for proper statistical averaging. Hence, the current continuum calculations and proposed empirical model are not appropriate to estimate the surface charging of nanopattern sizes smaller than $\sim$2–3 nm. These size values mostly yield the $\lambda/D_R > 10$ case and were carried out for the purpose of observing the extent of charging behavior at its limits to properly define the proposed empirical model in the corresponding mathematical limits.

Current results proved that surface heterogeneity creates dominant effects on surface charge formations. While such behavior creates complications for many applications (such as AFM), it can also be advantageous for future technologies. Nano-engineered surfaces can be designed with desired surface charging for a specific task. Our results for a sample circular surface pattern can be directly used for surface patterning using nanoparticles. On the other end, AFM measurements should incorporate the surface charge influence of surface heterogeneity. Considering the physical heterogeneity aspect of roughness only results in a wrong estimation for the surface forces measured in an ionic solution.

Conclusion

This study characterized the charge density of patterned silica surfaces. In contrast to many studies which consider the surface charge independent of the surface topography, this study calculated the effects of surface structures on surface charging. Using the numerical solution of ionic equilibrium based on the PNP equation with charge regulation boundaries, we found that the surface charge density is not just a material property but is dependent on the size of the surface roughness in addition to the solution conditions. In this regard, we calculated the local surface charge density based on the local ionic concentrations for different scenarios such as various surface pattern sizes and solution parameters. Through such a systematic approach, we evaluated both the local and average surface charge density of the patterned surfaces and associated these with the EDL overlap and curvature effects developing on the surface pattern. In general, as the surface structure diameter decreased, EDL overlap developed in the pits of the surface pattern, decreasing the surface charge value of the affected regions, while the curvature effect developed at the tips of the pattern, increasing the corresponding local surface charges. Hence, the homogeneous surface charge assumption is very much invalid since charge values at the pits can be half and at the tips can be double the predictions for a flat surface. Furthermore, we characterized the simultaneous behavior of these two mechanisms creating opposite effects by defining and calculating an average charge value through a symmetrical surface pattern. For our simple representative pattern made of repeating circular dips and tips of identical size, decreases in the surface charge at the dips and increases at the tips cancel each other up to a certain value of the surface pattern size and ionic concentration and the average surface charge remains the same as the surface charge of a flat surface. Further characterization was performed by combining the effect of the pattern size and ionic condition as the overlap ratio (λ/D_R). As the overlap ratio reached and exceeded the value of 0.2, the average surface charge of a patterned surface became less than the flat surface predictions and decreased further up to a certain asymptotic value depending strongly on pH. By increasing the overlap ratio, the electric potential distribution over the patterned surface becomes less bumpy and/or becomes flatter, which is the physical mechanism behind the convergence of the average surface charge to an asymptote at the high overlap ratio limit. For such a case, a flatter boundary definition will be required to define the average surface charge effective on the surface, instead of the surface charge on the arc length path of the surface pattern. Based on this idea, we further measured the average electric potential on a line boundary condition passing through the tips of the surface pattern, which was found to converge to the flat surface charge at the high overlap ratio limit. Using the numerical results, a phenomenological model describing the deviation of the average charge density of a patterned/rough surface from the flat surface theory is developed. The proposed model extends the existing theory as a function of the surface pattern size, ionic concentration, pH and constants of surface charge group chemistry, successfully.

Conflicts of interest

There are no conflicts to declare.

Acknowledgements

This work was supported by the Scientific and Technological Research Council of Turkey (TÜBİTAK) under the Grant Number 118M710 and Izmir Institute of Technology Research Funds under the Grant Number 2017-IYTE-57. Authors also would like to thank the Center for Scientific Computation at Southern Methodist University.

References

1 M. Fuest, K. K. Rangharajan, C. Boone, A. T. Conlisk and S. Prakash, Cation Dependent Surface Charge Regulation in Gated Nanofluidic Devices, *Anal. Chem.*, 2017, **89**, 1593–1601.
2 A. T. Celebi, M. Barisik and A. Beskok, Surface charge-dependent transport of water in graphene nano-channels, *Microfluid. Nanofluid.*, 2018, **22**, 7.
3 X. Gao, A. Omosebi, N. Holubowitch, J. Landon and K. Liu, Capacitive Deionization Using Alternating Polarization: Effect of Surface Charge on Salt Removal, *Electrochim. Acta*, 2017, **233**, 249–255.
4 I. Larson, C. J. Drummond, D. Y. C. Chan and F. Grieser, Direct force measurements between titanium dioxide surfaces, *J. Am. Chem. Soc.*, 1993, **115**, 11885–11890.
5 A. Klaassen, F. Liu, D. van den Ende, F. Mugele and I. Siretanu, Impact of surface defects on the surface charge of gibbsite nanoparticles, *Nanoscale*, 2017, **9**, 4721–4729.
6 C. von Roemeling, W. Jiang, C. K. Chan, I. L. Weissman and B. Y. S. Kim, *Trends Biotechnol.*, 2017, **35**, 159–171.
7 B. J. Feinberg, J. C. Hsiao, J. Park, A. L. Zydney, W. H. Fissell and S. Roy, Silicon nanoporous membranes as a rigorous platform for validation of biomolecular transport models, *J. Membr. Sci.*, 2017, **536**, 44–51.
8 Y. Zhang, G. Wu, W. Si, J. Ma, Z. Yuan, X. Xie, L. Liu, J. Sha, D. Li and Y. Chen, Ionic current modulation from DNA translocation through nanopores under high ionic strength and concentration gradients, *Nanoscale*, 2016, 930–939.
9 G. Huang, K. Willems, M. Soskine, C. Wloka and G. Maglia, Electro-osmotic capture and ionic discrimination of peptide and protein biomarkers with FraC nanopores, *Nat. Commun.*, 2017, **8**, 935.
10 E. Priyadarshini and N. Pradhan, *Sens. Actuators, B*, 2017, **238**, 888–902.
11 S. Brosel-Oliu, D. Galyamin, N. Abramova, F. X. Muñoz-Pascual and A. Bratov, Impedimetric label-free sensor for specific bacteria endotoxin detection by surface charge registration, *Electrochim. Acta*, 2017, **243**, 142–151.
12 R. F. Probstein, *Physicochemical hydrodynamics: an introduction*, John Wiley & Sons, 2005.
13 J. H. Masliyah and S. Bhattacharjee, *Electrokinetic and colloid transport phenomena*, John Wiley & Sons, 2006.
14 M. Kobayashi, F. Juillerat, P. Galletto, P. Bowen and M. Borkovec, Aggregation and charging of colloidal silica particles: effect of particle size, *Langmuir*, 2005, **21**, 5761–5769.
15 M. Barisik, S. Atalay, A. Beskok and S. Z. Qian, Size Dependent Surface Charge Properties of Silica Nanoparticles, *J. Phys. Chem. C*, 2014, **118**, 1836–1842.
16 F. Borghi, V. Vyas, A. Podestà and P. Milani, Nanoscale Roughness and Morphology Affect the IsoElectric Point of Titania Surfaces, *PLoS One*, 2013, **8**, e68655.
17 J. F. L. Duval, F. A. M. Leermakers and H. P. Van Leeuwen, Electrostatic interactions between double layers: Influence of surface roughness, regulation, and chemical heterogeneities, *Langmuir*, 2004, **20**, 5052–5065.
18 X. Yang and G. Zhang, The effect of an electrical double layer on the voltammetric performance of nanoscale interdigitated electrodes: a simulation study, *Nanotechnology*, 2008, **19**, 465504.
19 L. C. Hsu, J. Fang, D. A. Borca-Tasciuc, R. W. Worobo and C. I. Moraru, Effect of micro- and nanoscale topography on the adhesion of bacterial cells to solid surfaces, *Appl. Environ. Microbiol.*, 2013, **79**, 2703–2712.
20 O. Rzhepishevska, S. Hakobyan, R. Ruhal, J. Gautrot, D. Barbero and M. Ramstedt, The surface charge of anti-bacterial coatings alters motility and biofilm architecture, *Biomater. Sci.*, 2013, **1**, 589.
21 A. L. Božič, From discrete to continuous description of spherical surface charge distributions, *Soft Matter*, 2018, **14**, 1149–1161.
22 M. A. Blanco and V. K. Shen, Effect of the surface charge distribution on the fluid phase behavior of charged colloids and proteins, *J. Chem. Phys.*, 2016, **145**, 155102.
23 A. I. Abrikosov, B. Stenqvist and M. Lund, Steering patchy particles using multivalent electrolytes, *Soft Matter*, 2017, **13**, 4591–4597.
24 E. Bianchi, P. D. J. van Oostrum, C. N. Likos and G. Kahl, *Curr. Opin. Colloid Interface Sci.*, 2017, **30**, 8–15.
25 A. D. Stroock and G. M. Whitesides, Controlling flows in microchannels with patterned surface charge and topography, *Acc. Chem. Res.*, 2003, **36**, 597–604.
26 K. Ward and Z. H. Fan, Mixing in microfluidic devices and enhancement methods, *J. Micromech. Microeng.*, 2015, **25**, 094001.
27 Y. Yang, K. Webb, Y. Liu, K. Liu and Z. Nie, *Synthesis, Self-Assembly, and Applications of Amphiphilic Janus and Triblock Janus Nanoparticle Analogs*, World Scientific, 2017.
28 D. van Noort, *Bioreactors*, 2016.
29 M. Karle, S. K. Vashist, R. Zengerle and F. von Stetten, *Anal. Chim. Acta*, 2016, **929**, 1–22.
30 S. G. Elci, Y. Jiang, B. Yan, S. T. Kim, K. Saha, D. F. Moyano, G. Yesilbag Tonga, L. C. Jackson, V. M. Rotello and R. W. Vachet, Surface Charge Controls the Suborgan Biodistributions of Gold Nanoparticles, *ACS Nano*, 2016, **10**, 5536–5542.
31 E. Palleau, L. Ressier, L. Borowik and T. Mélin, Numerical simulations for a quantitative analysis of AFM electrostatic nanopatterning on PMMA by Kelvin force microscopy, *Nanotechnology*, 2010, **21**, 225706.
32 J. P. Hoogenboom, D. L. J. Vossen, C. Faivre-Moskalenko, M. Dogterom and A. van Blaaderen, Patterning surfaces

with colloidal particles using optical tweezers, *Appl. Phys. Lett.*, 2002, **80**, 4828–4830.
33 R. Parthasarathy, P. A. Cripe and J. T. Groves, Electrostatically driven spatial patterns in lipid membrane composition, *Phys. Rev. Lett.*, 2005, **95**, 048101.
34 M. Sayin and R. Dahint, Formation of charge-nanopatterned templates with flexible geometry via layer by layer deposition of polyelectrolytes for directed self-assembly of gold nanoparticles, *Nanotechnology*, 2017, **28**, 135303.
35 R. M. Fillion, A. R. Riahi and A. Edrisy, A review of icing prevention in photovoltaic devices by surface engineering, *Renewable Sustainable Energy Rev.*, 2014, **32**, 797–809.
36 L. Zhang, N. Zhao and J. Xu, Fabrication and application of superhydrophilic surfaces: a review, *J. Adhes. Sci. Technol.*, 2014, **28**, 769–790.
37 A. Koklu, A. Mansoorifar and A. Beskok, Self-Similar Interfacial Impedance of Electrodes in High Conductivity Media, *Anal. Chem.*, 2017, **89**, 12533–12540.
38 P. Zhang and S. Wang, Designing fractal nanostructured biointerfaces for biomedical applications, *ChemPhysChem*, 2014, **15**, 1550–1561.
39 B. Derjaguin and L. Landau, The theory of stability of highly charged lyophobic sols and coalescence of highly charged particles in electrolyte solutions, *Acta Physicochim. URSS*, 1941, **14**, 58.
40 E. J. W. Verwey, Theory of the stability of lyophobic colloids, *J. Phys. Chem.*, 1947, **51**, 631–636.
41 J. T. G. Overbeek and E. J. W. Verwey, *Theory of the Stability of Lyophobic Colloids: The interaction of Sol Particles Having an Electric Double Layer*, Elsevier, New York, 1948.
42 E. M. V. Hoek, S. Bhattacharjee and M. Elimelech, Effect of membrane surface roughness on colloid-membrane DLVO interactions, *Langmuir*, 2003, **19**, 4836–4847.
43 X. Huang, S. Bhattacharjee and E. M. V. Hoek, Is surface roughness a 'scapegoat' or a primary factor when defining particle-substrate interactions?, *Langmuir*, 2010, **26**, 2528–2537.
44 M. Bendersky and J. M. Davis, DLVO interaction of colloidal particles with topographically and chemically heterogeneous surfaces, *J. Colloid Interface Sci.*, 2011, **353**, 87–97.
45 N. Kumar, C. Zhao, A. Klaassen, D. Van den Ende, F. Mugele and I. Siretanu, Characterization of the surface charge distribution on kaolinite particles using high resolution atomic force microscopy, *Geochim. Cosmochim. Acta*, 2016, **175**, 100–112.
46 C. Zhao, D. Ebeling, I. Siretanu, D. van den Ende and F. Mugele, Extracting local surface charges and charge regulation behavior from atomic force microscopy measurements at heterogeneous solid-electrolyte interfaces, *Nanoscale*, 2015, **7**, 16298–16311.
47 G. Trefalt, S. H. Behrens and M. Borkovec, Charge Regulation in the Electrical Double Layer: Ion Adsorption and Surface Interactions, *Langmuir*, 2016, **32**, 380–400.
48 B. W. Ninham and V. A. Parsegian, Electrostatic potential between surfaces bearing ionizable groups in ionic equilibrium with physiologic saline solution, *J. Theor. Biol.*, 1971, **31**, 405–428.
49 V. E. Shubin and P. Kékicheff, Electrical Double Layer Structure Revisited via a Surface Force Apparatus: Mica Interfaces in Lithium Nitrate Solutions, *J. Colloid Interface Sci.*, 1993, **155**, 108–123.
50 J. P. Chapel, Electrolyte Species Dependent Hydration Forces between Silica Surfaces, *Langmuir*, 1994, **10**, 4237–4243.
51 M. Dishon, O. Zohar and U. Sivan, From repulsion to attraction and back to repulsion: the effect of NaCl, KCl, and CsCl on the force between silica surfaces in aqueous solution, *Langmuir*, 2009, **25**, 2831–2836.
52 I. Popa, P. Sinha, M. Finessi, P. Maroni, G. Papastavrou and M. Borkovec, Importance of charge regulation in attractive double-layer forces between dissimilar surfaces, *Phys. Rev. Lett.*, 2010, **104**, 228301.
53 K. Da Huang and R. J. Yang, Electrokinetic behaviour of overlapped electric double layers in nanofluidic channels, *Nanotechnology*, 2007, **18**, 115701.
54 A. Golovnev and S. Trimper, Steady state solution of the Poisson-Nernst-Planck equations, *Phys. Lett. A*, 2010, **374**, 2886–2889.
55 R. Nosrati, M. Hadigol, M. Raisee and A. Nourbakhsh, Numerical modeling of electroosmotic nanoflows with overlapped electric double layer, *J. Comput. Theor. Nanosci.*, 2012, **9**, 2228–2239.
56 J. K. Holt, H. G. Park, Y. Wang, M. Stadermann, A. B. Artyukhin, C. P. Grigoropoulos, A. Noy and O. Bakajin, Fast mass transport through sub-2-nanometer carbon nanotubes, *Science*, 2006, **312**, 1034–1037.
57 H. Verweij, M. C. Schillo and J. Li, Fast mass transport through carbon nanotube membranes, *Small*, 2007, **3**, 1996–2004.
58 S. Atalay, M. Barisik, A. Beskok and S. Qian, Surface charge of a nanoparticle interacting with a flat substrate, *J. Phys. Chem. C*, 2014, **118**, 10927–10935.
59 G. Karniadakis, A. Beskok and N. Aluru, *Microflows and nanoflows*, Springer, New York, 2005.
60 D. Li, *Electrokinetics In Microfluidics*, Elsevier/Academic Press, 2004.
61 S. Qian and Y. Ai, *Electrokinetic Particle Transport In Micro-/Nanofluidics*, CRC Press, Boca Raton, 2012.
62 M. Polat and H. Polat, Analytical solution of Poisson-Boltzmann equation for interacting plates of arbitrary potentials and same sign, *J. Colloid Interface Sci.*, 2010, **341**, 178–185.
63 Y. Ma, Y. S. Su, S. Qian and L. H. Yeh, Analytical model for surface-charge-governed nanochannel conductance, *Sens. Actuators, B*, 2017, **247**, 697–705.
64 W. Qu and D. Li, A model for overlapped EDL fields, *J. Colloid Interface Sci.*, 2000, **224**, 397–407.
65 C. L. Ren, Y. Hu, D. Li and C. Werner, A new model for the electrical double layer interaction between two surfaces in aqueous solutions, *J. Adhes.*, 2004, **80**, 831–849.
66 B. J. Kirby, *Micro-Nanoscale Fluid Mechanics Transport in Microfluidic Devices*, Cornell University, New York, 2010.
67 Y.-J. Oh, A. L. Garcia, D. N. Petsev, G. P. Lopez, S. R. J. Brueck, C. F. Ivory and S. M. Han, Effect of wall–molecule

interactions on electrokinetic transport of charged molecules in nanofluidic channels during FET flow control, *Lab Chip*, 2009, **9**, 1601.

68 M. Zhang, L. H. Yeh, S. Qian, J. P. Hsu and S. W. Joo, DNA electrokinetic translocation through a nanopore: local permittivity environment effect, *J. Phys. Chem. C*, 2012, **116**, 4793–4801.

69 D. Jing and B. Bhushan, Electroviscous effect on fluid drag in a microchannel with large zeta potential, *Beilstein J. Nanotechnol.*, 2015, **6**, 2207–2216.

70 M. A. Brown, M. Arrigoni, F. Héroguel, A. Beloqui Redondo, L. Giordano, J. A. Van Bokhoven and G. Pacchioni, PH dependent electronic and geometric structures at the water-silica nanoparticle interface, *J. Phys. Chem. C*, 2014, **118**, 29007–29016.

71 Y. Duval, J. A. Mielczarski, O. S. Pokrovsky, E. Mielczarski and J. J. Ehrhardt, Evidence of the existence of three types of species at the quartz-aqueous solution interface at pH 0-10: XPS surface group quantification and surface complexation modeling, *J. Phys. Chem. B*, 2002, **106**, 2937–2945.

72 M. A. Brown, A. Beloqui Redondo, M. Sterrer, B. Winter, G. Pacchioni, Z. Abbas and J. A. Van Bokhoven, Measure of surface potential at the aqueous-oxide nanoparticle interface by XPS from a liquid microjet, *Nano Lett.*, 2013, **13**, 5403–5407.

73 Y. Achdou, O. Pironneau and F. Valentin, Effective Boundary Conditions for Laminar Flows over Periodic Rough Boundaries, *J. Comput. Phys.*, 1998, **147**, 187–218.

74 S. Veran, Y. Aspa and M. Quintard, Effective boundary conditions for rough reactive walls in laminar boundary layers, *Int. J. Heat Mass Transfer*, 2009, **52**, 3712–3725.

75 J. Guo, S. Veran-Tissoires and M. Quintard, Effective surface and boundary conditions for heterogeneous surfaces with mixed boundary conditions, *J. Comput. Phys.*, 2016, **305**, 942–963.

76 T. Sen and M. Barisik, Size dependent surface charge properties of silica nano-channels: double layer overlap and inlet/outlet effects, *Phys. Chem. Chem. Phys.*, 2018, **20**, 16719–16728.

77 M. Kosmulski, *Surface Charging and Points of Zero Charge*, CRC Press, Boca Raton, 2009.